Electrochemical and Photochemical Reduction of CO2 Catalyzed by Re(I) Complexes Carrying Local Proton Sources

Electrochemical and Photochemical Reduction of CO_2 Catalyzed by Re(I) Complexes Carrying Local Proton Sources

Laura Rotundo,[a] Claudio Garino,[a] Emanuele Priola,[a] Daniele Sassone,[a] Heng Rao,[b] Bing Ma,[b] Marc Robert,[b] Jan Fiedler,[c] Roberto Gobetto[a] and Carlo Nervi*[a]*

[a] University of Torino, Department of Chemistry, via P. Giuria 7, 10125 Torino, Italy.

[b] Université Paris Diderot, Sorbonne Paris Cité, Laboratoire d'Electrochimie Moléculaire, UMR 7591 CNRS, 15 rue Jean-Antoine de Baïf, F-75205 Paris Cedex 13, France

[c] The Czech Academy of Sciences, J. Heyrovský Institute of Physical Chemistry, Dolejškova 3, 18223 Prague, Czech Republic

KEYWORDS. Electrochemistry, Photochemistry, CO_2 Reduction, Manganese, Rhenium.

ABSTRACT.

The novel rhenium complexes *fac*-Re(pdbpy)$(CO)_3$Cl (pdbpy = 4-phenyl-6-(phenyl-2,6-diol)-2,2'-bipyridine), **1**, and *fac*-Re(ptbpy)$(CO)_3$Cl (ptbpy = 4-phenyl-6-(phenyl-3,4,5-triol)-2,2'-bipyridine), **2**, have been synthesized and the single crystal X-Ray diffraction (SC-XRD) structure of **1** solved. The electrochemical behaviors of the complexes in acetonitrile under Ar and their catalytic performances for CO_2 reduction with added water and MeOH are discussed. A detailed IR spectroelectrochemical study under Ar and CO_2 atmospheres coupled with DFT calculations allows the identification of reduced species and the interpretation of the reduction mechanisms. Comparison between the rhenium complexes and the corresponding Mn derivatives Mn(pdbpy)$(CO)_3$Br, **3**, and Mn(ptbpy)$(CO)_3$Br, **4**, has been also considered. Finally, photo-stimulated conversion of the CO_2 was investigated with catalysts (**1**, **3**-**4**) under visible light irradiation (λ > 420

nm) in acetonitrile as solvent. Remarkably, **1** and **3** catalysts were active towards CO_2: producing formate with good selectivity and turnover number (TON). For example, **3** gives 62% selectivity for $HCOO^-$ and a TON of 80 and the Re compound **1** gives 74% selectivity for $HCOO^-$ and a TON of 86.

Introduction.

The overall world energy demand is constantly increasing, as well as the anthropogenic emissions of CO_2, its concentration in the atmosphere, and the associated environmental ravages. Undoubtedly the catalytic conversion of CO_2 is an attractive option that may allow producing chemicals and fuels upon energy storage, and that would help mitigating greenhouse effects in the mid-term (if the gas conversion could be achieved at the Gt scale, which remains currently unachieved).[1, 2] Worldwide energy data show that solar energy production by photovoltaics underwent a remarkable growth during last years, thus favouring the ongoing process of the long and complicated transition from fossil fuels to renewable energy.[3] However, the approach to produce sunlight energy in form of electricity still lacks from the point of view of high-density, long-term stability and suffers its intermittent nature and yet unsolved storage issue. The sunlight energy storage/conversion problem has not a unique and definitive solution, so that efforts in broadening the type of methodologies of the approaches should be pursued. Electrochemical processes driven by solar photovoltaic or direct photochemical reductions of CO_2 are recently undergoing an impressive upsurge of interests, in the hope to establish an efficient and reliable artificial carbon-cycle as energy vector for solar energy conversion.[4-9]

The choice of an efficient and selective catalyst for electrochemical reduction of CO_2 is mandatory.[2] While heterogeneous electrocatalysis is a promising approach in terms of durability, stability and improved TON efficiencies,[10-12] a rational approach based on the design of efficient homogeneous catalyst still has several benefits,[13, 14] including the possibility to covalently attach the molecular catalysts on the electrode surface.[15] While this paper was under evaluation, Mn and Re catalysts for CO_2 electrochemical reduction were chemically bonded on different electrode surfaces,[16, 17] and new Cu and Mn photocatalysts employed,[18] displaying very interesting conversions and TONs. In the search of efficient homogeneous catalysts for CO_2 reduction many groups explored organometallic complexes,[19-23] including alternatives to Re bpy-type complexes.[24-27] Deronzier and co-workers replaced Re with Mn,[28] and later we extended the concept of local proton source (first applied to iron porphyrins[29]) to Mn.[30-32] Ready (entropically) available local protons greatly enhance the catalytic

activity of CO_2 reduction. The previously synthesized complex **3**, carrying the pdbpy ligand (Scheme 1), generates formate via metal hydride species,[30, 31] in addition to the classical CO production, even in anhydrous acetonitrile. A significant improvement of the catalytic activities has been observed introducing the charge through space effect on iron porphyrins, both in electro-[33] and photo-catalysis.[34] However, the local proton source approach, albeit not fully understood, still has some advantages (sometimes unexpected as in the case of water oxidation[35]), like the possibility to change and tune the selectivity. In this paper, whose aim is to highlight differences between Mn and Re complexes carrying the same ligand, we explore the photo- and electro-catalytic activities of novel Re complexes (**1** and **2)** with pdbpy and ptbpy ligands (Scheme 1) and report the mechanism for the CO_2 catalytic reduction. We also report for the first time the photocatalytic activities of Mn complexes **3** and **4**. Comparison with the better-known corresponding Mn complexes helps in the understanding of the catalytic activities of such type of catalysts for homogeneous CO_2 reduction.

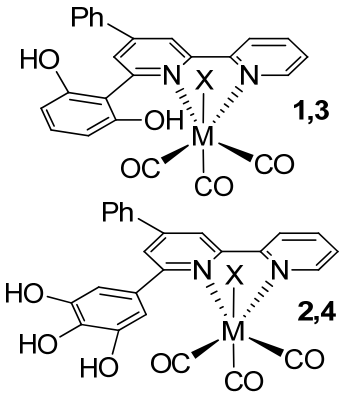

Scheme 1. Complexes investigated. (M=Re, X=Cl): **1**, Re(pdbpy)$(CO)_3$Cl; **2**, Re(ptbpy)$(CO)_3$Cl; (M=Mn, X=Br); **3**, Mn(pdbpy)$(CO)_3$Br; **4**: Mn(ptbpy)$(CO)_3$Br

Results and Discussion

Synthesis and structure

The novel rhenium complexes *fac*-Re(pdbpy)$(CO)_3$Cl (pdbpy = 4-phenyl-6-(phenyl-2,6-diol)-2,2'-bipyridine), **1** and *fac*-Re(ptbpy)$(CO)_3$Cl (ptbpy=4-phenyl-6-(phenyl-3,4,5-triol)-2,2-bipyridine), **2**, have been synthesized according to the procedure reported in the experimental section. Single-crystal X-Ray diffraction data of **1** has been obtained from yellow prismatic crystal, grown by slow evaporation under dark conditions

from a toluene/dichloromethane 1:1 solution. Compound **1** (Fig. 1a) crystallizes in a triclinic centrosymmetric $P\bar{1}$ space group. The metallic center has a slightly distorted octahedral geometry. The phenyl group in the 4' position of the ligand is almost coplanar with the aromatic bpy system (torsional angle of 32°), but the ellipsoids show a weak barrier to rotation. The diphenolic ring in the 6' position is instead nearly perpendicular to the α,α'-diimine plane (dihedral angle of 72.5°). This part of the structure is more ordered because of the presence of intramolecular hydrogen bond interaction with the chlorine bonded to the central metallic atom (d O5-H5…Cl1 = 3.102(10) Å, see Table S1). The overall packing of the molecular complex shows a multiplicity of weak hydrogens bonds and is stabilized by the presence of channels running along an axis filled by disordered toluene molecules that show C-H….π interactions (Figs. 1b and S1).

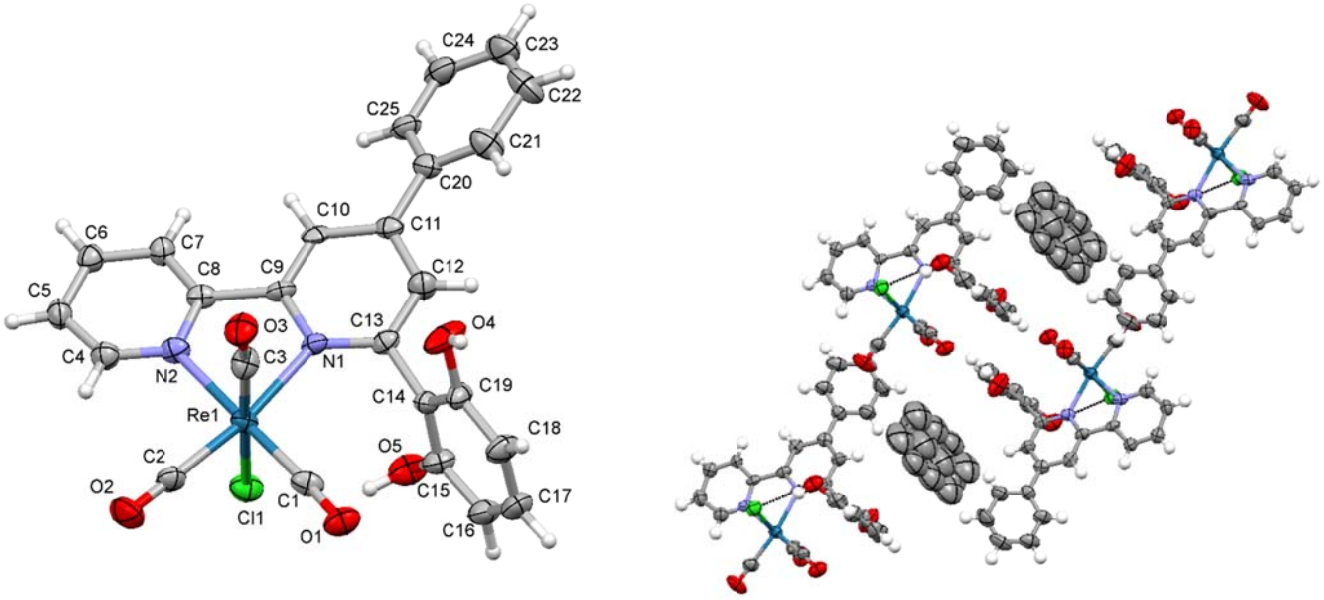

a) **b)**

Figure 1. Molecular structure of **1** from X-Ray single crystal diffraction (a) and representation of axial structural channels (b).

Cyclic Voltammetry

The electrochemical behaviour of **1** in anhydrous MeCN under Ar atmosphere (Fig. 2) resembles that of a common Re(bpy)$(CO)_3$Cl system.[24, 36] The $0/1^-$ reduction of **1** ($E° = –1.30$ V vs. Ag/AgCl) is chemically and electrochemically reversible, localized on the organic ligand with a non-negligible contribution of the Re metal.[37] The radical anion is usually stable in CV time scale, but in certain conditions and solvents Re(bpy-type)$(CO)_3$Cl radical anions may release Cl^-.[36] The $1^-/2^-$ reduction of **1** is chemically irreversible ($E_p = –1.59$ V vs. Ag/AgCl) and forms, after Cl^- dissociation, the intermediate penta-coordinated anion, $[Re(pdbpy)(CO)_3]^-$

acting as a precursor for CO_2 binding and subsequent reduction. The third process at more negative potentials is commonly assigned to a ligand-centred reduction. The broad reoxidation process observed after the second reduction and located between –0.5 and –0.8 V is due to adsorbed species on the electrode surface, since the current peak is proportional to the scan rate (for example see Fig. S2 at 100V/s).[38, 39]

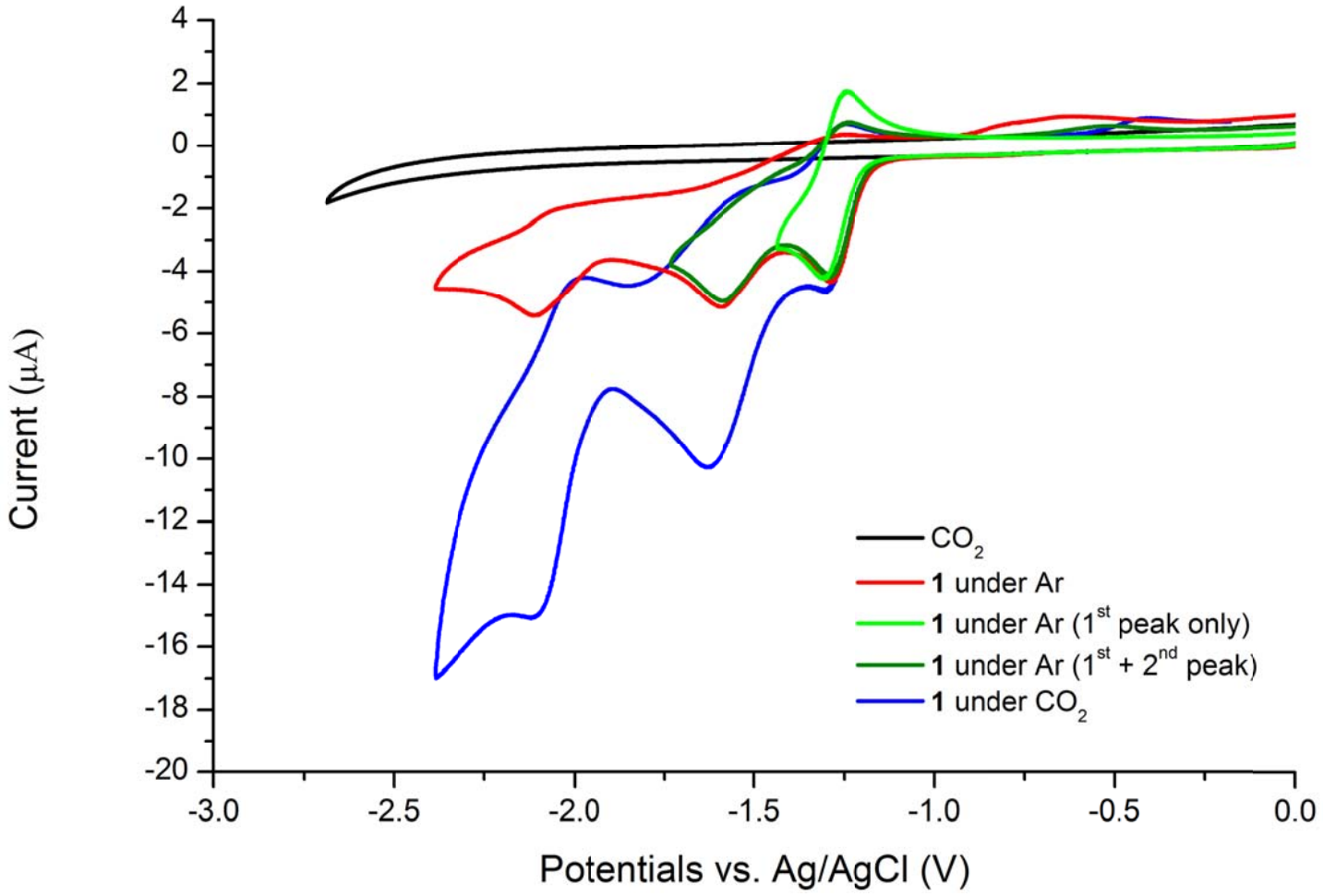

Figure 2. Cyclic voltammograms of 1 mM solution of **1** in MeCN / 0.1 M Bu_4NPF_6 at glassy carbon electrode, scan rate 200 mV/s. The black line is the electrolyte saturated with CO_2.

The reversibility of the $0/1^-$ reduction of **1** (see also Fig.S3) suggests that the release of Cl^- only occurs after the second electron transfer. This is nicely highlighted by relaxed geometry scan of the Re–Cl bond performed by DFT calculations on the radical anion $\mathbf{1}^-$ and the dianion $\mathbf{1}^{2-}$. Re–Cl bonds in the optimized structures of $\mathbf{1}^-$, $\mathbf{1}^{2-}$, $[Re(bpy)(CO)_3Cl]^-$ and $[Re(bpy)(CO)_3Cl]^{2-}$ are 2.779, 2.913, 2.776 and 4.609 Å, respectively, showing clearly the weakening of the Re-Cl bond after 2e reduction. The dissociation of Cl^- in MeCN as solvent requires 32.0 and only 1.7 kJ/mol for $\mathbf{1}^-$ and $\mathbf{1}^{2-}$, respectively (Fig. S4). The energetic barrier for the dissociation of the monoanion $[Re(bpy)(CO)_3Cl]^-$ is 40.1 kJ/mol, while it is barrierless in the dianion $[Re(bpy)(CO)_3Cl]^{2-}$ (leading to an optimized geometry in which the Re-Cl bond, 4.609 Å, is already broken). Thus, the calculations suggest

that pdbpy in $\mathbf{1}^-$ slightly facilitates the release of Cl^- from the complex, when compared to $[Re(bpy)(CO)_3Cl]^-$ in the same conditions. Equally important is the fact that release occurs from the doubly reduced species with very small barrier.

The CV of complex **1** in anhydrous MeCN under CO_2 atmosphere exhibits a small catalytic activity (increased current) already at the first reduction peak ($E_p = -1.30$V, Fig. 3). This is a notable difference from the other bipyridine-based rhenium catalysts, where the catalytic activity is observed in CV only at the second reduction peak.[20, 24]

The catalytic performance of **1** has been also investigated with the addition of two different external Brønsted acids: H_2O and MeOH. CVs in Figure 3 show that the addition of 5% of the two acids enhances the reactivity of **1** with CO_2 on the first and particularly on the second peak.

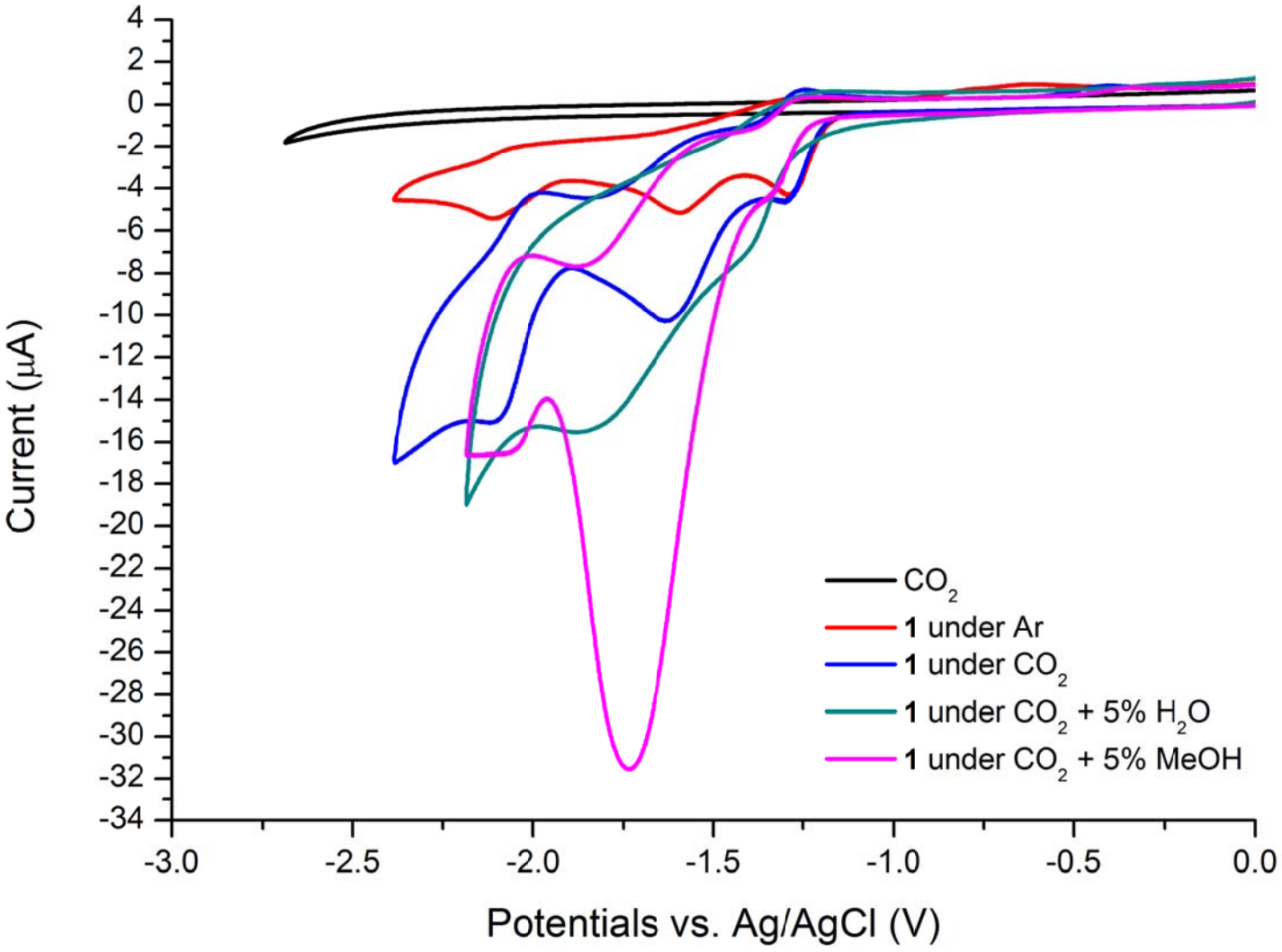

Figure 3. Cyclic voltammograms of 1 mM solutions of **1** in MeCN / 0.1 M Bu_4NPF_6 at 200 mV/s; black line is the background under CO_2.

Cyclic voltammetry of **2** Re(ptbpy)$(CO)_3$Cl, under Ar in anhydrous MeCN (Fig.4) exhibits three consecutive reduction processes. The first peak (at E_p= –1.38 V vs. Ag/AgCl) corresponds to the formation of the radical anion $[Re(ptbpy)(CO)_3Cl]^{\bullet-}$, and differently from **1**, shows a certain degree of chemical irreversibility (higher scan rates improves the reversibility). We were unable to completely remove water from compound **2** (a little amount of water has been always found during NMR characterization), resulting in a less reversible $0/1^-$ reduction, as well as altering the CV under CO_2. Furthermore, reproducibility of the CVs was an issue on GCE (glassy carbon electrode) because of the adsorption of reduction products or side-products causing an inactivation of the electrode surface. Similarly to **1**, two other reduction peaks are seen at –1.77 and –2.13 V vs. Ag/AgCl.

The electrochemical behavior of **2** in anhydrous MeCN under CO_2 atmosphere (Fig. 4) shows a net catalysis already at the first reduction peak. As mentioned above, this is due to small amounts of water retained in the more hydrophilic solid sample of **2**. Significant improvement is observed when MeOH or large amount (5%) of water are added. The CV peak currents decrease after consecutive CVs, but GCE cleaning restores the original CV with high catalytic current.

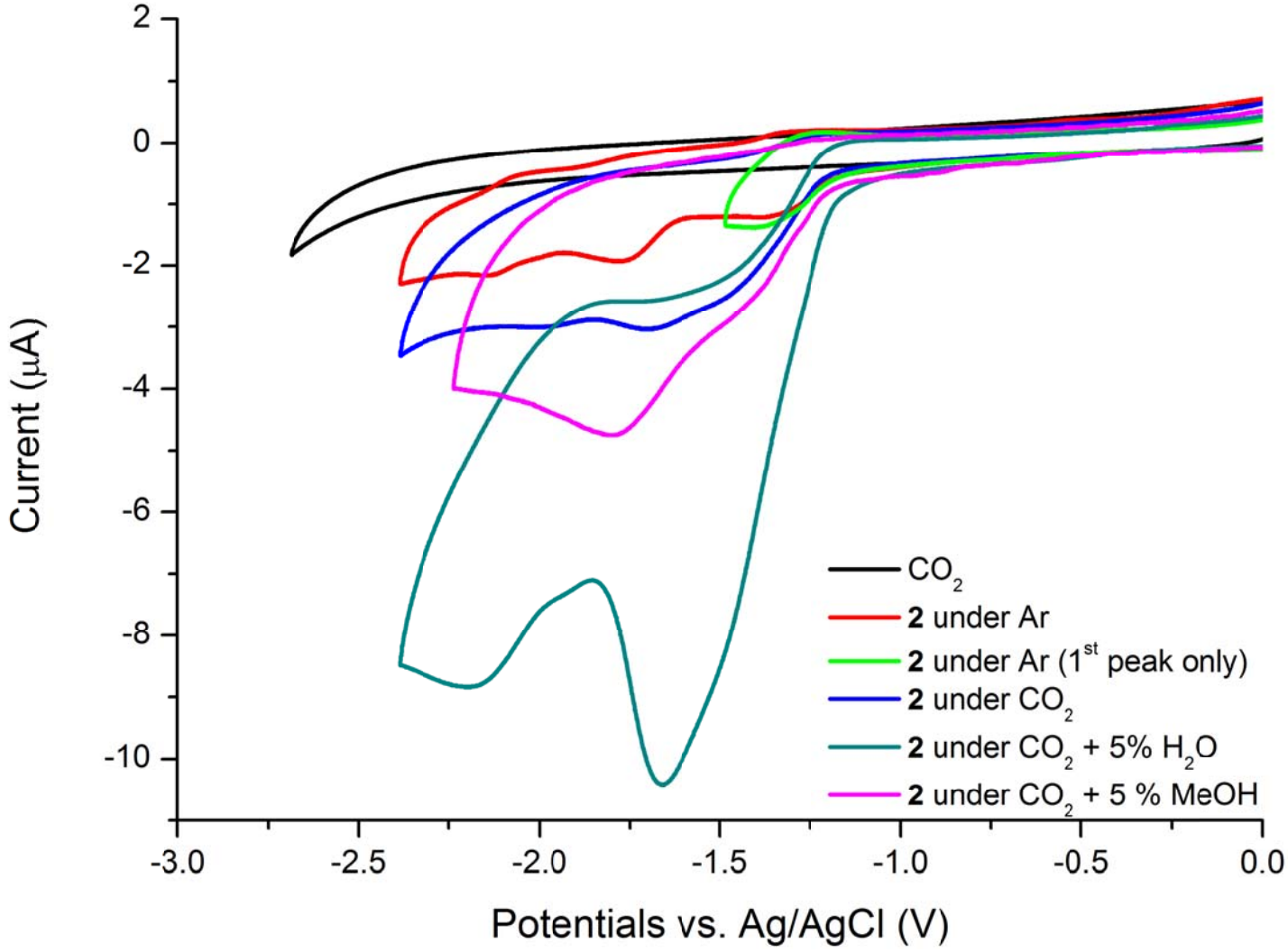

Figure 4. CVs of a 0.5 mM MeCN solution of **2** at 200 mV/s under Ar (red and green curve), under CO_2 (blue), under CO_2 and 5% H_2O (navy) and under CO_2 and 5% MeOH (violet) at a glassy carbon electrode

Spectroelectrochemistry in optically transparent thin-layer electrode (OTTLE) cell and DFT calculations of spectral bands

Infrared spectroelectrochemistry (IR-SEC) of complex **1** in acetonitrile under Ar was performed so as to monitor the spectral changes of the CO stretching bands (ν_{CO}). For all IR-SEC figures the arrows indicate the growing and decreasing of the corresponding bands. DFT calculations have been used as complementary tool for the assignment of the products and intermediate species observed during IR-SEC bulk electrolysis under Ar. Figure 5 shows spectral changes during the potential scan up of –1.4 V vs. Ag/AgCl, i.e just after the first reduction peak. As a main feature a progressive loss of the ν_{CO} stretches of complex **1** (2023, 1918 and 1901 cm^{-1}) was observed along with the simultaneous growth of a new species (**1d**, in Table 1 and Scheme 2) characterized by IR absorptions at 2010, 1901 and 1879 cm^{-1}. The reduction in the OTTLE cell is irreversible (the reversed potential scan does not lead to the original spectrum), however this is not in contradiction with the

CV reversibility, because of the quite different time scales of CV and IR-SEC.[31] The longer time scale in IR-SEC experiments allows ligand exchange between Cl^- and a solvent molecule and the subsequent rearrangement to **1d** (Scheme 2). The decrease in intensity of the OH stretches at 3318 cm^{-1} (inset in Fig. 5) suggests that **1d** is a species originated from a reductive single deprotonation of the starting complex **1**, i.e. **1d** is formulated as ([$Re(CO)_3$(pdbpy−H^+)]). A similar reductive deprotonation has already been observed for the analogous Mn complex.[31]

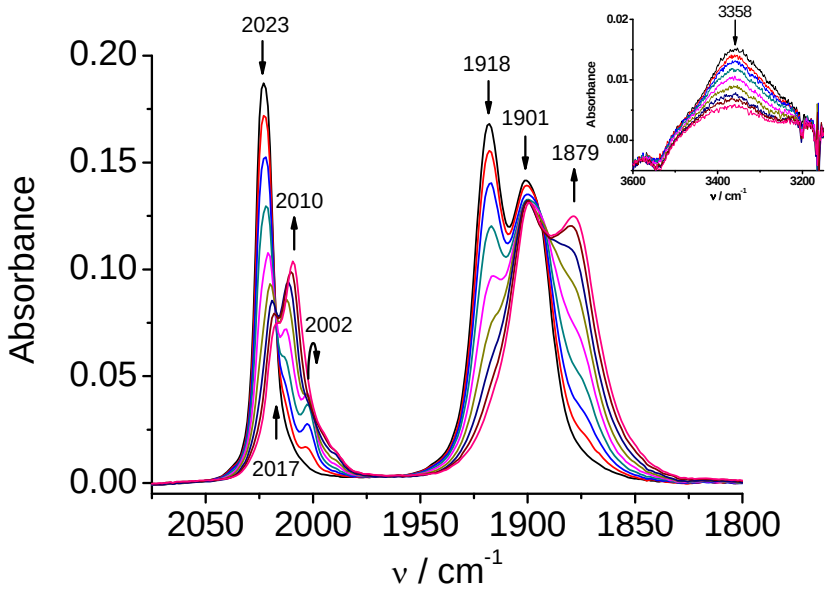

Figure 5. IR-Spectroelectrochemical reduction of a 2.9 mM solution of **1** in MeCN / 0.1 M Bu_4NPF_6 under Ar at the first reduction wave (final potential –1.4 V vs. Ag/AgCl). The inset shows the decrease of ν_{OH}.

The transition from **1** to **1d** (bands at 2010, 1901 and 1879 cm^{-1}, see Fig. 5 and Scheme 2) proceeds via the formation of other intermediate species, as revealed by the presence of ν_{CO} at 2017 and 2002 cm^{-1}, which finally converge into the peak at 2010 cm^{-1}. Two possible intermediates could be involved in the transformation.[20, 40] The band at 2002 cm^{-1} is attributed the radical anion **1a** (1998 cm^{-1} observed for the analogous complex with unsubstituted bipyridine),[40] and the band at 2017 cm^{-1} could be due to the corresponding radical **1b** obtained by substitution of Cl^- by MeCN (2011 cm^{-1} observed for bpy analogue).[40] In conclusion, **1d** is the predominant species at the end of the first reduction in IR-SEC time scale experiments.

IR-SEC experiments with Et_4NCl (tetraethylammonium chloride) have been performed with the aim of stabilizing the radical anion **1a** by decreasing the rate of Cl^- loss. The IR-SEC (Fig. 6) shows slightly shifted

absorptions, and the starting ν_{CO} at 2020, 1916 and 1894 cm^{-1} of **1** are transformed, after reduction at the first wave, into ν_{CO} at 2006, 1993, 1894 and 1874 cm^{-1}. These four absorption bands can be seen as a sum of IR spectra of the species **1d** and additional product(s). The band 1993 can be ascribed to the anion $[Re(CO)_3(pdbpy)MeCN]^-$ (**1c**) which is formed in limited amount due to close reduction potentials of **1** and **1b.** Formation of analogous $[Re(CO)_3(bpy)MeCN]^-$ with bands 1986, 1868, 1852 cm^{-1} was observed during reduction of $[Re(CO)_3(bpy)Cl]$ in similar conditions.[40] IR bands at 2002, 1891, 1871(sh) cm^{-1} appearing in the early stage of the electrolysis can be assigned to the radical anion **1a** (DFT computed at 1999, 1892 and 1875 cm^{-1}) formed as intermediate. Also, a band at 2017 cm^{-1} attributable to the neutral radical **1b** (DFT computed at 2017, 1917, 1899 cm^{-1}) appears temporarily. The corresponding experimental values for $[Re(bpy)(CO)_3Cl]^{\bullet-}$ and $[Re(bpy)(CO)_3(MeCN)]^{\bullet}$ in MeCN were reported to be 1998, 1885, 1866 cm^{-1} and 2011, 1895(br) cm^{-1}, respectively,[40] in excellent agreement with calculations. The presence of Et_4NCl partially suppresses the Cl^- dissociation, but eventually in a longer time scale the 1e reduction still ends in the conversion to **1d**.

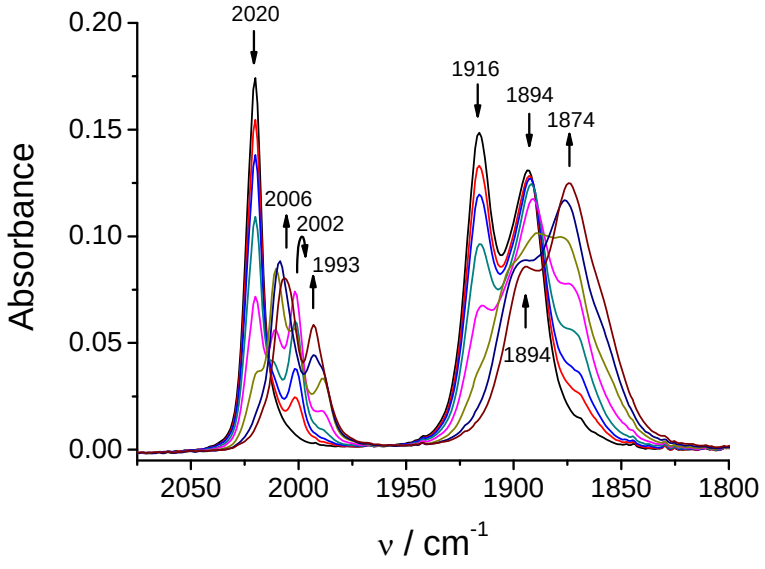

Figure 6. IR spectroelectrochemistry of **1** in MeCN/0.1 M Et_4NCl under Ar at the first reduction wave (final potential –1.4 V vs. Ag/AgCl).

Complex	Experimental ν_{CO} (cm^{-1})	DFT (cm^{-1})
[Re(pdbpy)(CO)$_3$Cl] (**1**)	2023, 1918, 1901	2021, 1921, 1902
[Re(bpy)(CO)$_3$Cl]	2021, 1914, 1897[a]	2017, 1911, 1901
[Re(pdbpy)(CO)$_3$Cl]$^{\bullet-}$ (**1a**)	2002, 1891, 1871sh	1999, 1892, 1875
[Re(pdbpy)(CO)$_3$MeCN]$^{\bullet}$ (**1b**)	2017	2017, 1917, 1899
[Re(bpy)(CO)$_3$MeCN]$^{\bullet}$	2011, 1895(br)[a]	2007, 1898, 1892
[Re(pdbpy)(CO)$_3$MeCN]$^{-}$ (**1c**)	1993	1989, 1890, 1869
[Re(pdbpy–H)(CO)$_3$] (**1d**)	2010, 1901, 1879	2008, 1901, 1888
[Re(pdbpy–H)(CO)$_3$]$^{\bullet-}$ (**1g**)	1985, 1865, 1850	1986, 1870, 1861
[Re(pdbpy–2H)(CO)$_3$]$^{-}$ (**1h**)	2002, 1890	1997, 1888, 1871

[a] from ref.[40]

Table 1. Selected experimental (IR-SEC) and calculated ν_{CO} frequencies of **1** and other related complexes from IR spectroelectrochemistry in MeCN and DFT computed data.

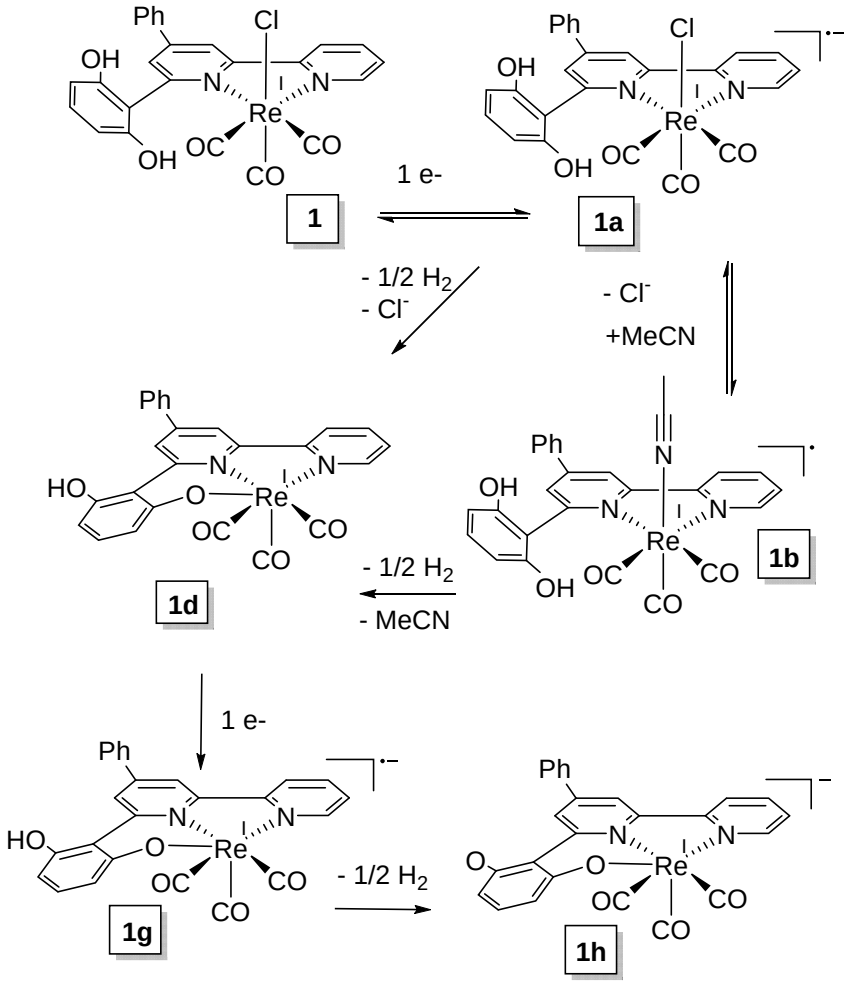

Scheme 2. Electrochemical reductive mechanism for **1** under Ar.

IR-SEC of **1** in anhydrous acetonitrile under Ar at the second reduction wave (Fig. 7) shows that the bands at 2010, 1901 and 1879 cm^{-1} are replaced by 2002, 1985, 1890, 1865 and 1850 cm^{-1}. The species (**1d**), formed after the first reduction, undergoes further reduction (Scheme 2) leading to species (**1g**) (1985, 1868 and 1850 cm^{-1}) which could subsequently generate (**1h**) (2002 and 1890 cm^{-1}) after loss of ½ H_2 (where the charge may now formally be localized on the oxygen atom).

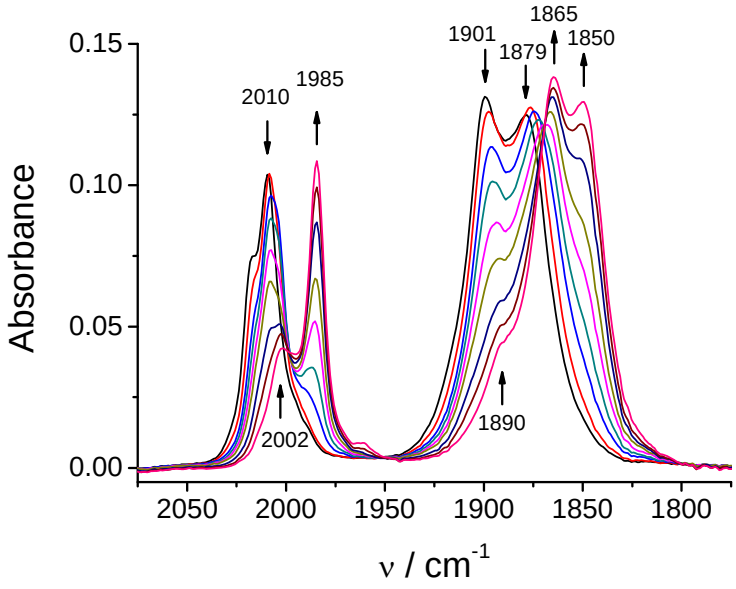

Figure 7. IR spectroelectrochemistry of **1** in MeCN/0.1 M Bu_4NPF_6 under Ar at the second reduction wave (final potential –1.7 V vs. Ag/AgCl).

IR-SEC spectra of **1** in MeCN under CO_2-saturated solutions at the first reduction peak are quite similar to those obtained under Ar atmosphere, with a small exception of the growth of a peak at 1684 cm^{-1} (Fig. S5), assigned to the presence of HCO_3^-/CO_3^{2-} species.[40] During the reduction at the second peak under CO_2, IR-SEC at early stage (Fig. S6) rapidly reach a steady-state situation (Fig. 8): the bands at 2010, 1901 and 1875 cm^{-1}, close to those found for (**1d**) (2010, 1901, 1879 cm^{-1}; Fig. 5, Table 1), remain almost unchanged, while new strong ν_{CO} bands at 1684, 1645 (HCO_3^-/CO_3^{2-} system[40]) increase continuously. Under these conditions stationary concentration of (**1g**) is too small to be detected: only a weak shoulder of its strong absorption is present at 1985 cm^{-1} (Figs. S6 and Fig. 8).

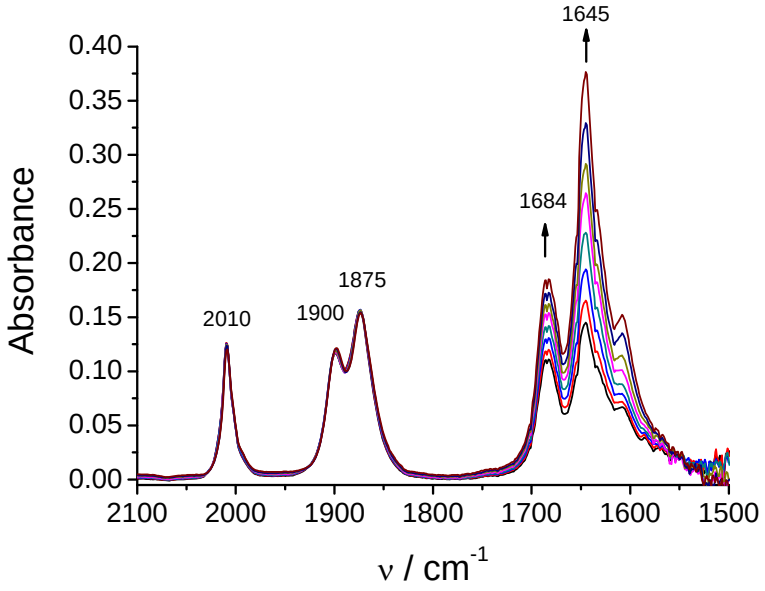

Figure 8. IR spectroelectrochemistry of **1** in MeCN/0.1 M Bu_4NPF_6 under CO_2: steady state established at continuing electrolysis at the second reduction wave (final potential –1.7V vs Ag/AgCl).

It is interesting to underline that passing from **3** (Mn(pdbpy)) to **1** (Re(pdbpy)), the same ligand has an important effect on the electrochemical properties: the hydride formation in Re is apparently supressed. No formate production has been observed during exhaustive electrolysis (see below).

The active catalytic species are supposed to be the radical anion (**1g**) and/or the anion (**1h**), obtained by loss of ½ H_2 from (**1g**). By analogy with the Muckerman and Schaefer mechanism,[41] CO production may involve a carbonate-bridged complex. In that paper the authors highlighted the affinity of Re with O atom, allowing the CO_2 insertion into the carbonate-bridged complex. O atom in **1** is close to Re, resulting in the formation of a Re-O bond of the entropically favoured intermediate (**1d**), which is reduced to **1g** (Scheme 3). Preliminary DFT calculations suggest that an alternative mechanistic pathway, not involving carbonate-bridged intermediate, may also be possible for **1**. A CO_2 insertion into the Re-O bond of the reduced species **1g** (or **1h**) is feasible, and results into carbonate species (Figure S7) that may further react with a second CO_2 molecule leading to CO and CO_3^{2-} as products.

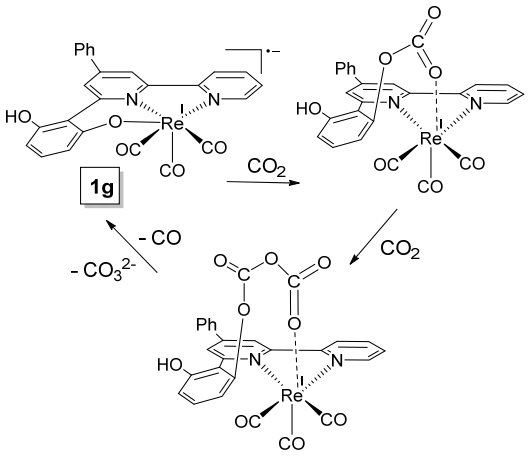

Scheme 3. Proposed mechanism of the electrochemical reduction of CO_2 into CO with **1** as catalyst (similar to the mechanism proposed in reference [41]).

Controlled Potential Electrolysis (CPE)

Bulk electrolysis with **1** and **2** under CO_2 were performed upon setting the potential at values slightly negative to the first and second reductions, with and without added Brønsted acids (water and methanol, 5%). Table 2 summarizes the results obtained during these CPE experiments. A CO_2 flow of 30 mL min^{-1} was kept constant during the experiments, CO and H_2 were identified by gas chromatography, and formate, if present, was assessed by NMR spectroscopy at the end of the experiments. In MeCN/H_2O at the first reduction (–1.5 V vs. Ag/AgCl, Fig.9a) the TON_{CO} for **1** (7.5) is lower than the TON_{CO} of the corresponding Mn complex **3** (28).[31] The fact that TON_{CO} for **2** (E = –1.6 V vs. Ag/AgCl) increases to 11.4 also suggests that **1** is a less active electrocatalyst. The situation is inverted at the second peak potential, where TON_{CO} of **1** rises to 14.1 (E = –1.7 V vs. Ag/AgCl, Fig.9b), whereas TON_{CO} of **2** drops to a very low value of 2 (E = –1.9 V vs. Ag/AgCl) (Table 4). This is due to the above-mentioned adsorption phenomena onto the GCE that quickly passivate the electrode surface. As in cyclic voltammetry experiments, simple mechanical cleaning of the electrode could restore the catalytic activity. Figure 9 also highlights the good electrocatalytic properties of **1** over time.

Complex	E [V]	T [min]	Acid [5%]	TON_{CO}	η_{CO} [%]
1	–1.5	120	-	2.2	60
		270	H_2O	7.5	76
		270	MeOH	4.0	52
1	–1.7	150	-	2.9	49
		300	H_2O	14.1	88
		240	MeOH	4.4	64
2	–1.6	270	-	6.6	98
		250	H_2O	11.4	100
		170	MeOH	5.9	100
2	–1.9	170	-	3.7	70
		100	H_2O	2	70
		130	MeOH	0.7	60

Table 2. TON and faradic efficiencies (η) upon CPE (applied potential E in V vs. Ag/AgCl) of solutions containing **1** or **2** (0.5 mM) in 0.1M Bu_4NPF_6/MeCN in the presence of Brønsted acids (5%v).

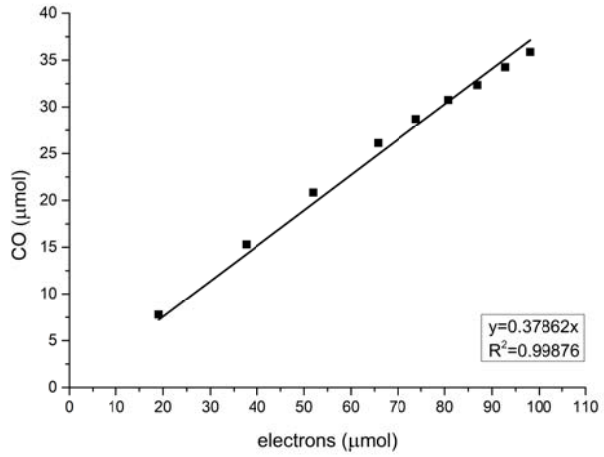

a)

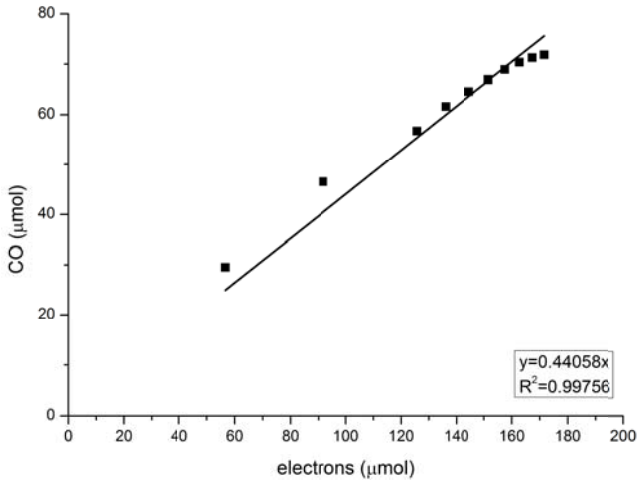

b)

Figure 9. Catalytic CO production from CO_2 as a function of the charge during CPE carried out in MeCN solutions of **1** (0.5 mM) at: a) –1.5 V with 5%v H_2O; b) –1.7 V with 5%v H_2O.

Photocatalytic Experiments

Some photo-stimulated conversion of the CO_2 was investigated with catalysts **1**, **3** and **4**, whereas for complex **2** extensive decomposition prevented to obtain reproducible data. All experiments were driven under visible light irradiation (λ > 420 nm) in acetonitrile as solvent. *fac*-(tris-(2-phenylpyridine))iridium(III) ($Ir(ppy)_3$) was used as a photosensitizer and trimethylamine was employed as a sacrificial electron donor. The catalysts were active towards CO_2 with excellent selectivity for CO_2 reduction (Table 5 and Figure 10), ranging from 89% to 97% depending on the experimental conditions, and a maximum total TON of 143 for the

production of CO and $HCOO^-$. All experiments were repeated two times and gave reproducible results. Blank experiments confirmed that all components of the systems were necessary for catalytic activity and the reduction products were issued from the carbon dioxide. With all the components of the systems but in the absence of light, no products were formed. Under argon atmosphere, no products were formed either except traces of CO (TON < 3, which can be explained by carbonyl release from the catalyst) and H_2, and the same conclusions hold true in the absence of sacrificial donor or of sensitizer. Finally, no products at all were formed in the absence of the catalysts. Turnover numbers were obtained by dividing the mol number of product by the initial quantity of catalyst, similarly to electrochemical experiments. Only small amounts of H_2 were obtained as by-product (2.5% in the case of **3** and 3.3% with **1**). Remarkably, both Mn and Re catalysts were able to produce formate with good selectivity and turnover. For example, **3** gives 62% selectivity for $HCOO^-$ and a TON of 80 and the Re compound **1** gives 74% selectivity for $HCOO^-$ and a TON of 86. In the presence of 0.5 M H_2O, the formation of CO_2 reduction products was enhanced (Table 3), with a maximum TON for formate close to 100 with both **1** and **3**. Emission quenching experiments showed efficient quenching reaction between **1** or **3** and the photo-excited $Ir(ppy)_3$ ($Ir(ppy)_3$*) with a second order rate constant of $k_q \approx 5.5 \times 10^9$ M^{-1} s^{-1} and 3.9×10^9 M^{-1} s^{-1} respectively (see Figures S12-S13), which supports an oxidative electron transfer from $Ir(ppy)_3$* to the catalysts. This result falls in line with the fact that standard redox potential of the excited sensitizer (-1.73 V vs. SCE) is negative enough to reduce all catalysts to their active states. The change in product distribution as compared to electrochemical results may originate from a mechanistic change; being beyond the scope of this contribution, it will be studied in a future report.

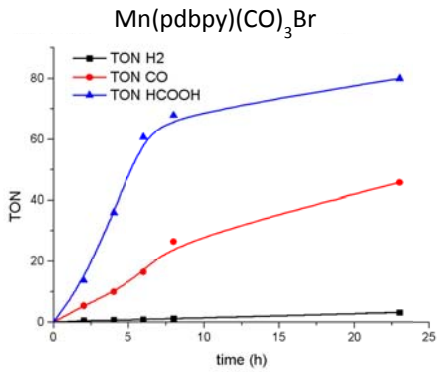

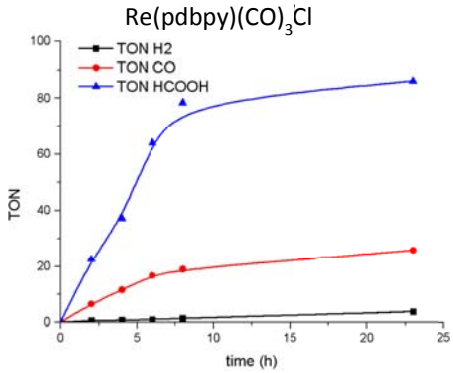

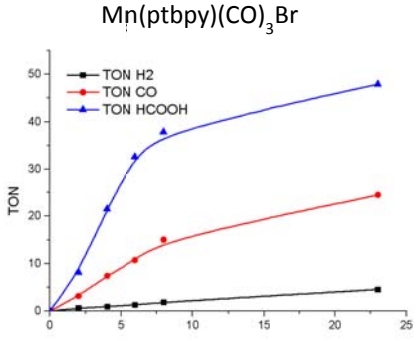

Figure 10. TON values vs. time during photochemical irradiation experiments for Mn(pdbpy)$(CO)_3$Br (**3**), Re(pdbpy)$(CO)_3$Cl (**1**) and Mn(ptbpy)$(CO)_3$Br (**4**). Reaction conditions: 5 μM Cat. + 0.2mM $Ir(ppy)_3$ + 0.05M TEA + MeCN/CO_2 + >420 nm light

	TON_{H2} (CS)	TON_{CO} (CS)	TON_{HCOO-} (CS)
Re(pdbpy) (**1**)	4 (3.3%) 12.5 (8%)[a]	26 (22.3%) 53 (34%)[a]	86 (74.4%) 90 (58%)[a]
Mn(pdbpy) (**3**)	3 (2.5%) 16 (11.2%)[a]	46 (35.5%) 30 (21%)[a]	80 (62.0%) 97 (67.8%)[a]
Mn(ptbpy) (**4**)	5 (5.7%)	24 (30.9%)	50 (63.4%)

Table 3. TON from photo-irradiation (24h) of solutions of 1, 3 and 4 (5 μM) in MeCN in the presence of $Ir(ppy)_3$ (0.2 mM) and TEA (0.05 M). a: in the presence of 0.5 M H_2O as an acid co-substrate.

Concluding Remarks

This contribution provides further insights into the role of a local proton source in CO_2 reduction catalysts by investigating the electrochemical and spectroscopic features of the novel rhenium complexes Re(pdbpy)$(CO)_3$Cl, **1**, and Re(ptbpy)$(CO)_3$Cl (ptbpy = 4-phenyl-6-(phenyl-3,4,5-triol)-2,2'-bipyridine), **2** under inert atmosphere as well as under CO_2. Comparison between the rhenium complexes and the corresponding Mn derivatives Mn(pdbpy)$(CO)_3$Br, **3**, and Mn(ptbpy)$(CO)_3$Br, **4,** has been also considered. Although the electrochemical behaviour of **1** in anhydrous MeCN under Ar atmosphere resembles that of a common Re(bpy)$(CO)_3$Cl system, DFT calculations suggest that pdbpy in $\mathbf{1}^-$ slightly facilitates the release of Cl^- from the complex, when compared to $[Re(bpy)(CO)_3Cl]^-$ in the same conditions. Another interesting difference of **1** with respect to other bipyridine-based rhenium catalysts is the presence of small catalytic activity already at the first reduction peak in anhydrous MeCN under CO_2 atmosphere. We surmise that the catalytic activity after the first reduction is associated with the lower energy required for the release of Cl^-. The addition of H_2O and MeOH enhances the reactivity of **1** with CO_2 on the first and particularly on the second reduction peak. Compound **2** shows similar behavior at first CV cycles, but in a longer time the adsorption phenomena alter the catalysis. The hygroscopic behavior of **2** does not allow a clean comparison.

Spectroelectrochemical (IR and UV/Vis) investigation coupled with DFT calculations allows the identification of reduced species and interpretation of the reduction mechanisms. Controlled Potential Electrolysis of **1** and **2** under CO_2 in MeCN/H_2O at the first reduction (–1.5 V vs. Ag/AgCl) shows that the TON_{CO} of **1** (7.5) is lower than the TON_{CO} of **2** (E = –1.6 V vs. Ag/AgCl), which is probably altered by the water retained in **2**. At this potential there are no evidences of adsorption phenomena by **2**. Conversely, at the second peak potential, where increased catalytic performances are expected, TON_{CO} of **1** rises to 14.1 (E = –1.7 V vs. Ag/AgCl), whereas TON_{CO} of **2** drops to a very low value of 2 (E = –1.9 V vs. Ag/AgCl) due to passivation of the electrode surface. These data apparently suggest that the local proton source effects are more pronounced for Mn in comparison with Re complexes.

In reductive electrochemical experiments it is interesting to note that while Mn(pdbpy) gives the hydride with subsequent production of formate, the corresponding Re(pdbpy) undergoes a different reaction pathway and no formate is produced upon catalytic cycles. It is only during photochemical experiments, under different reaction conditions, that significant formate TON values are obtained, thus showing that the coordination of the pdbpy ligand to Re and Mn alter the selectivity of the reaction products.

Experimental Section

NMR spectra were recorded on a JEOL Eclipse 400 spectrometer (^1H operating frequency 400 MHz) at 298 K. ^1H and ^{13}C chemical shifts are reported relative to TMS (δ=0) and referenced against solvent residual peaks.

IR-ATR spectra were collected on a Fourier transform Equinox 55 (Bruker) spectrophotometer equipped with an ATR device; resolution was set at 2 cm^{-1} for all spectra. A spectral range of 400–4000 cm^{-1} was scanned, using KBr as a beam splitter.

The pdbpy and tpbpy ligands were synthesized accordingly to the Kröhnke reaction between an α,β-unsaturated substrate (chalcone) and pyridinium salt carried out in methanol in presence of large excess of ammonium acetate, as already reported by some of us.[30, 31] All reagents were purchased from Sigma-Aldrich and used as received. Solvents were freshly distilled and purged with Ar before use.

Synthesis of [Re(pdbpy)(CO)$_3$Cl] (1). [$Re(CO)_5Cl$] (0.500 mmol, 1 equiv) and pdbpy (0.501 mmol, 1.01 eq) were refluxed for 3 hours in anhydrous toluene (20 mL) while stirring. Alternatively, reaction proceeded in a sealed flask for microwave reactor and evolved at 130 °C for an hour. After cooling of the reaction mixture to

room temperature, petroleum ether was added to precipitate the yellow product, which was then centrifuged, filtered and washed once with cold diethyl ether (yield 75 %).

^{1}H-NMR: [400 MHz, $(CD_3)_2SO$]: δ/ppm 9.60 (s, 1H), 9.56 (s, 1H), 9.05 (t, J = 8.8 Hz, 2H), 9.01 (s, 1H), 8.35 (t, J = 7.4 Hz, 1H), 8.11 (d, J = 7.8 Hz, 2H), 7.85 (s, 1H), 7.73 (t, J = 6.3 Hz, 1H), 7.60 (m, 3H), 7.15 (t, J = 7.5 Hz, 1H:), 6.45 (t, J = 7.5 Hz, 2H). (Fig. S11a)

^{13}C-NMR: [400 MHz, $(CD_3)_2SO$]: δ/ppm = 198.87, 194.61, 191.23, 160.25, 157.47, 156.99, 156.70, 156.58, 153.00, 150.25, 140.24, 135.61, 131.10, 129.89, 129.46, 128.77, 128.19, 126.73, 125.46, 120.09, 118.03, 107.35, 106.64.

IR-ATR: ν/cm^{-1} = 3244, 2022, 1911, 1885.

Synthesis of [Re(ptbpy)(CO)$_3$Cl] (2). The reaction proceeded similarly to [Re(pdbpy)(CO)$_3$Cl]. ([Re(CO)$_5$Cl] (0.500 mmol, 1 equiv) and ptbpy (0.501 mmol, 1.01 eq) were refluxed for 3 hours in anhydrous toluene (20 mL) while stirring (yields 70%).

^{1}H-NMR: [400 MHz, $(CD_3)_2SO$]: δ/ppm =9.06 (d, J = 7.47 Hz, 2H), 8.96 (s, 1H), 8.35 (t, J = 8.57 Hz, 1H), 8.15-8.18 (m, 2H),7.96 (s, 1H), 7.75 (t, J = 7.03, 1H), 7.59-7.62 (m, 3H), 6.54 (d, J= 27.97 Hz, 2H). (Fig.S11b).

^{13}C-NMR: [400 MHz, $(CD_3)_2SO$]: δ/ppm = 196.92, 194.41,191.76, 181.02, 164.59, 157.43, 156.86, 153.19, 150.47, 146.5, 140.28, 135.66, 135.61, 133.04, 131,29, 129.89, 128.38, 127.90, 125.96,124.86, 120.26, 109.34.

IR-ATR: ν/cm^{-1}: 3226, 2026, 1913, 1877.

The experimental setup is similar to that previously reported.[31] **Electrochemical experiments** were performed using a Metrohm Autolab 302n potentiostat; acetonitrile was freshly distilled and purged with argon before use, tetrabutylammonium hexafluorophosphate (Bu_4NPF_6, Sigma–Aldrich, 98%), employed as supporting electrolyte, was recrystallized twice from ethanol and dried before use. The reference electrode Ag/AgCl (KCl 3M) was employed. Under these experimental conditions the redox couple Fc^+/Fc is located at $E_{1/2}$= 0.35V (ΔE_p= 56mV).

DFT calculations were performed as previously reported,[31] employing the B3LYP method coupled with the basis set def2TZVP for heavy metals and def2SVP for lighter elements. **IR-SEC spectroelectrochemistry** were performed in a OTTLE cell,[42] analogously as previously reported.[31]

Quantitative analysis of CO_2 reduction products. CO was detected and quantified using an Agilent 490 Micro GC gas chromatograph equipped with a CP-Molsieve 5 Å columns, which was kept at 85°C and at a pressure of 21 psi, with a thermal conductivity detector. The carrier gas was He. The backflush vent option time was set to 4.5 s. A second module equipped with a CP-Molsieve 5 Å column using Ar as carrier gas was used for H_2 analysis. The gas inside the measurement cell was sampled for 30 s every three minutes to fill the Micro GC 10 μL sample loop, and eventually 500 nL were injected into the column for the analyses. We used Ar, He, CO_2 pure gases (>99.9995%) from Sapio for the operation, and two different certified standard concentrations of CO and H_2 in Ar matrix (Rivoira) for calibration (Fig. S8). Detection limits for CO and H_2 were 1 ppmv and 0.5 ppmv, respectively. Formate production was quantitatively evaluated using NMR spectroscopy.

Single-Crystal X-ray diffraction. Data for compound **1** have been collected on a Gemini R Ultra diffractometer using graphite-monochromated Mo Ka radiation (k = 0.71073 Å) with the ω-scan method. Cell parameters were retrieved using CrysAlisPro[43] software, and the same program has been used for performing data reduction, with corrections for Lorenz and polarizing effects. Scaling and absorption corrections were applied by the CrysAlisPro multi-scan technique. The structure was solved by Patterson Function using Sir2014[44] and refined with full-matrix least-squares on F^2 using SHELXL[45]. All non-hydrogen atoms were anisotropically refined. Hydrogen atoms were calculated and riding on the corresponding atom. Structural illustrations have been drawn with Mercury.[46] The crystallographic data for **1** have been deposited within the Cambridge Crystallographic Data Centre as supplementary publications under the CCDC number 1857181. This information can be obtained free of charge from the Cambridge Crystallographic Data Centre via www.ccdc.cam.ac.uk/data_request/cifcode CCDC.

Photocatalytic experiments. Irradiation of either CO_2- or argon-saturated 3.5 mL solution containing the catalyst, the photosensitizer and the sacrificial electron donor were conducted in a closed 1 cm × 1 cm quartz suprasil cuvette (Hellma 117.100F-QS) equipped with home-designed headspace glassware for further gaseous product quantification. A Newport LCS-100 solar simulator, equipped with an AM1.5 G standard filter allowing 1 Sun irradiance and combined with a Schott GG420 longpass filter and a 2-cm-long glass (OS) cell filled with deionized water to prevent catalyst absorbance and to cut off infrared and low ultraviolet, was used as the light source and was placed at right angle of the sample. In these experiments, gaseous products analysis

was performed with an Agilent Technology 7820A gas chromatography (GC) system set with a CarboPLOT P7 capillary column (25 m length and 25 mm inner diameter) and a thermal conductivity detector. Calibration curves for H_2 and CO were established separately. Formate was quantified with a Dionex ICS-1100 Ionic Chromatography System equipped with a IonPac AS15 column (KOH 20 mM as eluent). UV-Visible absorption spectra were recorded with an Analytik Jena Specord 600 spectrophotometer. Emission quenching measurements were conducted with a Cary Eclipse fluorescence spectrophotometer (Agilent Technologies), with the excitation wavelength set at 420 nm. Emission intensities used for the Stern-Volmer analysis were taken at 517 nm, *i.e.* the emission maximum of $Ir(ppy)_3$.

AUTHOR INFORMATION

Corresponding Authors

- Roberto Gobetto (roberto.gobetto@unito.it) and Carlo Nervi (carlo.nervi@unito.it), University of Torino, Department of Chemistry, via P. Giuria 7, 10125 Torino, Italy.

ACKNOWLEDGMENT

J.F. thanks the Czech Science Foundation (project 18-09848S) for support. H.R. and B. M. thank the China Scholarship Council for his PhD fellowship (CSC student number 201507040033 (H.R.) and 201707040042 (B.M.)). Partial financial support to M. R. from the Institut Universitaire de France (IUF) is gratefully acknowledged. PHOTORECARB (University of Torino and Compagnia di San Paolo) and CRT (Fondazione CRT, Ref. 2017.0812) projects are acknowledged.

REFERENCES

1. Qiao, J.; Liu, Y.; Hong, F.; Zhang, J., A review of catalysts for the electroreduction of carbon dioxide to produce low-carbon fuels. *Chem. Soc. Rev.* **2014,** *43*, 631-675.
2. Ronge, J.; Bosserez, T.; Martel, D.; Nervi, C.; Boarino, L.; Taulelle, F.; Decher, G.; Bordiga, S.; Martens, J. A., Monolithic cells for solar fuels. *Chem. Soc. Rev.* **2014,** *43*, 7963-7981.
3. Armaroli, N.; Balzani, V., Solar Electricity and Solar Fuels: Status and Perspectives in the Context of the Energy Transition. *Chem. Eur. J.* **2016,** *22*, 32-57.
4. Wang, J.-W.; Liu, W.-J.; Zhong, D.-C.; Lu, T.-B., Nickel complexes as molecular catalysts for water splitting and CO_2 reduction. *Coord. Chem. Rev.* **2019,** *378*, 237-261.
5. Sinopoli, A.; La Porte, N. T.; Martinez, J. F.; Wasielewski, M. R.; Sohail, M., Manganese carbonyl complexes for CO_2 reduction. *Coord. Chem. Rev.* **2018,** *365*, 60-74.
6. Kuramochi, Y.; Ishitani, O.; Ishida, H., Reaction mechanisms of catalytic photochemical CO_2 reduction using Re(I) and Ru(II) complexes. *Coord. Chem. Rev.* **2018,** *373*, 333-356.

7. Wang, J.-W.; Huang, H.-H.; Sun, J.-K.; Ouyang, T.; Zhong, D.-C.; Lu, T.-B., Electrocatalytic and Photocatalytic Reduction of CO_2 to CO by Cobalt(II) Tripodal Complexes: Low Overpotentials, High Efficiency and Selectivity. *ChemSusChem* **2018,** *11*, 1025-1031.
8. Wang, J.-W.; Huang, H.-H.; Sun, J.-K.; Zhong, D.-C.; Lu, T.-B., Syngas Production with a Highly-Robust Nickel(II) Homogeneous Electrocatalyst in a Water-Containing System. *ACS Catalysis* **2018,** *8*, 7612-7620.
9. Cao, L.-M.; Huang, H.-H.; Wang, J.-W.; Zhong, D.-C.; Lu, T.-B., The synergistic catalysis effect within a dinuclear nickel complex for efficient and selective electrocatalytic reduction of CO_2 to CO. *Green Chemistry* **2018,** *20*, 798-803.
10. Sun, C.; Rotundo, L.; Garino, C.; Nencini, L.; Yoon, S. S.; Gobetto, R.; Nervi, C., Electrochemical CO_2 Reduction at Glassy Carbon Electrodes Functionalized by Mn^I and Re^I Organometallic Complexes. *ChemPhysChem* **2017,** *18*, 3219-3229.
11. Sun, C.; Prosperini, S.; Quagliotto, P.; Viscardi, G.; Yoon, S. S.; Gobetto, R.; Nervi, C., Electrocatalytic reduction of CO_2 by thiophene-substituted rhenium(i) complexes and by their polymerized films. *Dalton Trans.* **2016,** *45*, 14678-88.
12. Sun, C.; Gobetto, R.; Nervi, C., Recent advances in catalytic CO_2 reduction by organometal complexes anchored on modified electrodes. *New J. Chem.* **2016,** *40*, 5656-5661.
13. Elgrishi, N.; Chambers, M. B.; Wang, X.; Fontecave, M., Molecular polypyridine-based metal complexes as catalysts for the reduction of CO_2. *Chem. Soc. Rev.* **2017,** *46*, 761-796.
14. Takeda, H.; Cometto, C.; Ishitani, O.; Robert, M., Electrons, Photons, Protons and Earth-Abundant Metal Complexes for Molecular Catalysis of CO_2 Reduction. *ACS Catalysis* **2017,** *7*, 70-88.
15. Sandroni, M.; Volpi, G.; Fiedler, J.; Buscaino, R.; Viscardi, G.; Milone, L.; Gobetto, R.; Nervi, C., Iridium and ruthenium complexes covalently bonded to carbon surfaces by means of electrochemical oxidation of aromatic amines. *Catal. Today* **2010,** *158*, 22-28.
16. Clark, M. L.; Ge, A.; Videla, P. E.; Rudshteyn, B.; Miller, C. J.; Song, J.; Batista, V. S.; Lian, T.; Kubiak, C. P., CO_2 Reduction Catalysts on Gold Electrode Surfaces Influenced by Large Electric Fields. *J. Am. Chem. Soc.* **2018,** *140*, 17643-17655.
17. Rotundo, L.; Filippi, J.; Gobetto, R.; Miller, H. A.; Rocca, R.; Nervi, C.; Vizza, F., Electrochemical CO_2 reduction in water at carbon cloth electrodes functionalized with a *fac*-Mn(apbpy)$(CO)_3$Br complex. *Chem. Commun.* **2019,** DOI: 10.1039/c8cc08385a.
18. Takeda, H.; Kamiyama, H.; Okamoto, K.; Irimajiri, M.; Mizutani, T.; Koike, K.; Sekine, A.; Ishitani, O., Highly Efficient and Robust Photocatalytic Systems for CO_2 Reduction Consisting of a Cu(I) Photosensitizer and Mn(I) Catalysts. *J. Am. Chem. Soc.* **2018,** *140*, 17241-17254.
19. Kumar, B.; Llorente, M.; Froehlich, J.; Dang, T.; Sathrum, A.; Kubiak, C. P., Photochemical and Photoelectrochemical Reduction of CO_2. *Annu. Rev. Phys. Chem.* **2012,** *63*, 541-569.
20. Machan, C. W.; Sampson, M. D.; Chabolla, S. A.; Dang, T.; Kubiak, C. P., Developing a Mechanistic Understanding of Molecular Electrocatalysts for CO_2 Reduction using Infrared Spectroelectrochemistry. *Organometallics* **2014,** *33*, 4550-4559.
21. Machan, C. W.; Stanton, C. J.; Vandezande, J. E.; Majetich, G. F.; Schaefer, H. F.; Kubiak, C. P.; Agarwal, J., Electrocatalytic Reduction of Carbon Dioxide by Mn(CN)(2,2′-bipyridine)$(CO)_3$: CN Coordination Alters Mechanism. *Inorg. Chem.* **2015,** *54*, 8849-8856.
22. Sampson, M. D.; Nguyen, A. D.; Grice, K. A.; Moore, C. E.; Rheingold, A. L.; Kubiak, C. P., Manganese Catalysts with Bulky Bipyridine Ligands for the Electrocatalytic Reduction of Carbon Dioxide: Eliminating Dimerization and Altering Catalysis. *J. Am. Chem. Soc.* **2014,** *136*, 5460-5471.
23. Riplinger, C.; Sampson, M. D.; Ritzmann, A. M.; Kubiak, C. P.; Carter, E. A., Mechanistic Contrasts between Manganese and Rhenium Bipyridine Electrocatalysts for the Reduction of Carbon Dioxide. *J. Am. Chem. Soc.* **2014,** *136*, 16285-16298.
24. Hawecker, J.; Lehn, J. M.; Ziessel, R., Electrocatalytic reduction of carbon dioxide mediated by Re(bpy)$(CO)_3$Cl (bipy = 2,2'-bipyridine). *J. Chem. Soc., Chem. Commun.* **1984**, 328-330.
25. Hawecker, J.; Lehn, J. M.; Ziessel, R., Efficient photochemical reduction of CO_2 to CO by visible light irradiation of systems containing Re(bipy)$(CO)_3$X or Ru$(bipy)_3^{2+}$-Co^{2+} combinations as homogeneous catalysts. *J. Chem. Soc., Chem. Commun.* **1983**, 536-538.
26. Smieja, J. M.; Kubiak, C. P., Re(bipy-^{t}Bu)$(CO)_3$Cl-improved Catalytic Activity for Reduction of Carbon Dioxide: IR-Spectroelectrochemical and Mechanistic Studies. *Inorg. Chem* **2010,** *49*, 9283-9289.

27. Smieja, J. M.; Sampson, M. D.; Grice, K. A.; Benson, E. E.; Froehlich, J. D.; Kubiak, C. P., Manganese as a Substitute for Rhenium in CO_2 Reduction Catalysts: The Importance of Acids. *Inorg. Chem* **2013,** *52*, 2484-2491.
28. Bourrez, M.; Molton, F.; Chardon-Noblat, S.; Deronzier, A., Mn(bipyridyl)$(CO)_3$Br : An Abundant Metal Carbonyl Complex as Efficient Electrocatalyst for CO_2 Reduction. *Angew. Chem. Int. Ed.* **2011,** *50*, 9903-9906.
29. Costentin, C.; Drouet, S.; Robert, M.; Saveant, J. M., A Local Proton Source Enhances CO_2 Electroreduction to CO by a Molecular Fe Catalyst. *Science* **2012,** *338*, 90-94.
30. Franco, F.; Cometto, C.; Ferrero Vallana, F.; Sordello, F.; Priola, E.; Minero, C.; Nervi, C.; Gobetto, R., A local proton source in a [Mn(bpy-R)$(CO)_3$Br]-type redox catalyst enables CO_2 reduction even in the absence of Brønsted acids. *Chem. Commun.* **2014,** *50*, 14670-14673.
31. Franco, F.; Cometto, C.; Nencini, L.; Barolo, C.; Sordello, F.; Minero, C.; Fiedler, J.; Robert, M.; Gobetto, R.; Nervi, C., Local Proton Source in Electrocatalytic CO_2 Reduction with [Mn(bpy-R)$(CO)_3$Br] Complexes. *Chem. Eur. J.* **2017,** *23*, 4782-4793.
32. Dubey, A.; Nencini, L.; Fayzullin, R. R.; Nervi, C.; Khusnutdinova, J. R., Bio-Inspired $Mn^{(I)}$ Complexes for the Hydrogenation of CO_2 to Formate and Formamide. *ACS Catalysis* **2017,** *7*, 3864-3868.
33. Azcarate, I.; Costentin, C.; Robert, M.; Savéant, J. M., Through-Space Charge Interaction Substituent Effects in Molecular Catalysis Leading to the Design of the Most Efficient Catalyst of CO_2-to-CO Electrochemical Conversion. *J. Am. Chem. Soc.* **2016,** *138*, 16639-16644.
34. Rao, H.; Schmidt, L. C.; Bonin, J.; Robert, M., Visible-light-driven methane formation from CO_2 with a molecular iron catalyst. *Nature* **2017,** *548*, 74-77.
35. Bucci, A.; Dunn, S.; Bellachioma, G.; Menendez Rodriguez, G.; Zuccaccia, C.; Nervi, C.; Macchioni, A., A Single Organoiridium Complex Generating Highly Active Catalysts for both Water Oxidation and NAD^+/NADH Transformations. *ACS Catalysis* **2017,** *7*, 7788-7796.
36. Sullivan, B. P.; Bolinger, C. M.; Conrad, D.; Vining, W. J.; Meyer, T. J., One-Electron and 2-Electron Pathways in the Electrocatalytic Reduction of CO_2 by Fac-Re(2,2'-Bipyridine)$(CO)_3$Cl. *J. Chem. Soc., Chem. Commun.* **1985**, 1414-1415.
37. Záliš, S.; Consani, C.; El Nahhas, A.; Cannizzo, A.; Chergui, M.; Hartl, F.; Vlcek, A., Origin of electronic absorption spectra of MLCT-excited and one-electron reduced 2,2 '-bipyridine and 1,10-phenanthroline complexes. *Inorg. Chim. Acta* **2011,** *374*, 578-585.
38. Bard, A. J.; Faulkner, L. R., *Electrochemical Methods*. 2nd Edition ed.; Wiley: New York, 2001.
39. Zanello, P.; Nervi, C.; Fabrizi De Biani, F., *Inorganic Electrochemistry. Theory, Practice and Application*. 2nd ed.; RSC: Cambridge, 2011.
40. Johnson, F. P. A.; George, M. W.; Hartl, F.; Turner, J. J., Electrocatalytic reduction of CO_2 using the complexes $[Re(bpy)(CO)_3L]^{(n)}$ (n=+1, L=$P(OEt)_3$, CH_3CN; n=0, L=Cl^-, $Otf^{(-)}$; bpy=2,2'-bipyridine; $Otf^{(-)}$=CF_3SO_3) as catalyst precursors: Infrared spectroelectrochemical investigation. *Organometallics* **1996,** *15*, 3374-3387.
41. Agarwal, J.; Fujita, E.; Schaefer, H. F.; Muckerman, J. T., Mechanisms for CO Production from CO_2 Using Reduced Rhenium Tricarbonyl Catalysts. *J. Am. Chem. Soc.* **2012,** *134*, 5180-5186.
42. Krejčik, M.; Daněk, M.; Hartl, F., Simple construction of an infrared optically transparent thin-layer electrochemical cell: Applications to the redox reactions of ferrocene, $Mn_2(CO)_{10}$ and $Mn(CO)_3$(3,5-di-*t*-butyl-catecholate)$^-$. *Journal of Electroanalytical Chemistry and Interfacial Electrochemistry* **1991,** *317*, 179-187.
43. Agilent *CrysAlisPro*, 1.171.37.31 (release 14-01-2014 CrysAlis171. NET, compiled Jan 14 2014, 18:38:05); Agilent Technologies, Yarnton, England2014.
44. Burla, M. C.; Caliandro, R.; Carrozzini, B.; Cascarano, G. L.; Cuocci, C.; Giacovazzo, C.; Mallamo, M.; Mazzone, A.; Polidori, G., Crystal structure determination and refinement via SIR2014. *J. Appl. Crystallogr.* **2015,** *48*, 306-309.
45. Sheldrick, G. M., Crystal structure refinement with SHELXL. *Acta Crystallogr. Sect. C: Cryst. Struct. Commun.* **2015,** *C71*, 3-8.
46. Macrae, C. F.; Edgington, P. R.; McCabe, P.; Pidcock, E.; Shields, G. P.; Taylor, R.; Towler, M.; van De Streek, J., Mercury: visualization and analysis of crystal structures. *J. Appl. Crystallogr.* **2006,** *39*, 453-457.

Table of Contents